UCRL 2923

UNCLASSIFIED

UNIVERSITY OF CALIFORNIA

Radiation Laboratory

TWO-WEEK LOAN COPY

This is a Library Circulating Copy which may be borrowed for two weeks. For a personal retention copy, call Tech. Info. Division, Ext. 5545

BERKELEY, CALIFORNIA

DISCLAIMER

This document was prepared as an account of work sponsored by the United States Government. While this document is believed to contain correct information, neither the United States Government nor any agency thereof, nor the Regents of the University of California, nor any of their employees, makes any warranty, express or implied, or assumes any legal responsibility for the accuracy, completeness, or usefulness of any information, apparatus, product, or process disclosed, or represents that its use would not infringe privately owned rights. Reference herein to any specific commercial product, process, or service by its trade name, trademark, manufacturer, or otherwise, does not necessarily constitute or imply its endorsement, recommendation, or favoring by the United States Government or any agency thereof, or the Regents of the University of California. The views and opinions of authors expressed herein do not necessarily state or reflect those of the United States Government or any agency thereof or the Regents of the University of California.

UCRL-2833
Unclassified Physics

UNIVERSITY OF CALIFORNIA
Radiation Laboratory
Berkeley, California

Contract No. W-7405-eng-48

SCATTERING AND ABSORPTION OF π^+-MESONS IN LEAD

George Saphir

(Thesis)

January 4, 1955

Printed for the U. S. Atomic Energy Commission

SCATTERING AND ABSORPTION OF π^+-MESONS IN LEAD

Contents

	Abstract	3
I.	Introduction	4
II.	Experimental Procedure	5
III.	Reduction of Data	9
	A. Scanning Procedure	9
	B. Meson Flux	9
	C. Elastic Scatters	11
	D. Inelastic Scatters	13
	E. Charge-Exchange Scatters	15
	F. Proton Events	16
	G. Stops	16
	H. Acceptance Criteria for Events	16
IV.	Results and Discussion	17
	A. Elastic Scattering	17
	B. Inelastic Scattering	19
	C. Charge-Exchange Scattering	20
	D. Absorption	21
	E. Analysis of Star Fragments	22
	F. Energy Dependence	28
V.	Summary	31
	Acknowledgments	31
	Appendices	32
	References	44

SCATTERING AND ABSORPTION OF π^+-MESONS IN LEAD

George Saphir

Radiation Laboratory, Department of Physics
University of California, Berkeley, California

January 4, 1955

ABSTRACT

The interactions of 50±15-Mev π^+-mesons in lead were investigated by means of a magnet cloud chamber containing a single 1/8-inch lead plate. The following cross sections were found: for elastic scattering greater than 40°, 252±36 mb; for star production, 852±82 mb; for charge-exchange scattering, 27±19 mb. Only one of the 52 observed scatters was inelastic. The elastic scattering has a minimum near 90°. The mean free path of π^+-mesons in nuclear matter, derived from the inelastic events and large-angle scatters in this experiment, is $(9.0 \pm 1.5) \times 10^{-13}$ cm. The results are compared with information from related experiments.

SCATTERING AND ABSORPTION OF π^+-MESONS IN LEAD

George Saphir

Radiation Laboratory, Department of Physics
University of California, Berkeley, California

January 4, 1955

I. INTRODUCTION

Meson scattering experiments are important aids in the study of nuclear forces and of the structure of nuclei. Because of its fundamental nature, scattering in hydrogen has claimed the most attention. Scattering by complex nuclei has only been done in a rather exploratory fashion, but the gaps are being filled in steadily.

Meson absorption cross sections of many elements have been measured at several energies. The details of the interactions, however, have been investigated primarily for light elements. The experiment reported here serves to furnish data on the interactions of π^+-mesons and lead.

A cloud chamber was used for this experiment because it permits the simultaneous investigation of several features of the meson-nuclear interactions. Of interest are: the angular distribution of the scattered mesons; the cross sections for inelastic scattering, charge-exchange scattering, and absorption; and the characteristics of the star fragments. Because these features impose conflicting requirements on the experimental arrangements, the actual experiment represents a compromise, which yields information on all these aspects with reasonable accuracy.

II. EXPERIMENTAL PROCEDURE

The procedure used in this experiment was very similar to that used by Tracy[1] and is therefore described only briefly.

Meson Beam

The mesons were produced in a 2-inch-thick polyethylene target placed in the electrostatically deflected proton beam of the 184-inch synchrocyclotron. The meson beam[2] was deflected away from the proton beam by means of a large electromagnet and passed through a hole in the concrete shielding. It then entered the cloud chamber located just outside the shielding. Fig. 1 shows the experimental arrangement.

Cloud Chamber

The expansion-type cloud chamber[3] is 22 inches in diameter and has a sensitive region 3.5 inches deep. It was filled with argon at 90 cm pressure and contained a vapor mixture of water and ethyl alcohol. The moisture was contained in a black gelatine coating on the piston. Across the center of the chamber was placed a 1/8-inch (actually 3.335 g/cm^2) lead plate covered with thin aluminum foil ($4.8 \times 10^{-3} g/cm^2$) to improve the illumination. The cloud chamber was situated in a large electromagnet[3] capable of producing fields up to 22 kilogauss. Fields of 5.18 and 7.33 kilogauss were used in this experiment because higher fields would have caused the radii of curvature of the meson paths to be too small for sufficient mesons to reach the lead plate, and would also have produced too much dispersion of the beam.

The cloud chamber was expanded once every 1.5 minutes just before the meson beam entered the chamber. Usually four pulses spaced 1/60 second apart were used. The lights were flashed 7/60 second after the last meson pulse.

Two runs were made to obtain the data of this experiment. In the first one most data were taken with the 5.18-kilogauss field and with the mesons entering nearly normal to the plate; additional data were obtained with the higher field, the mesons then entering the plate at about 15° from the normal. Because tracks emerging near 90° might

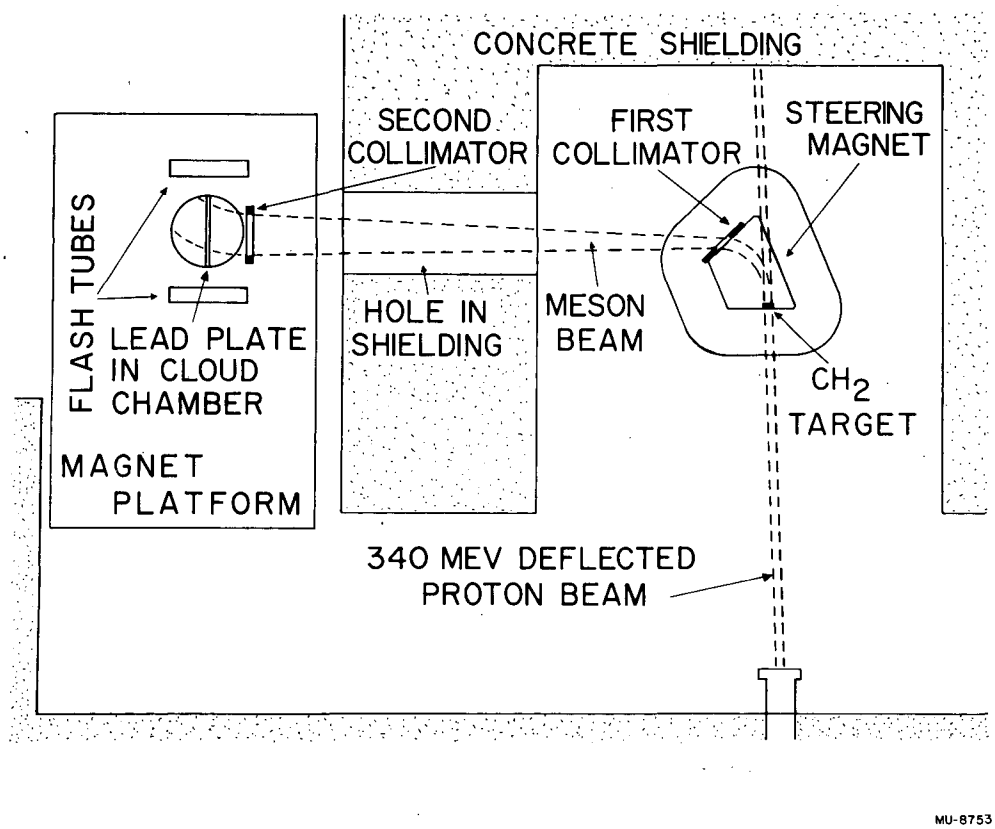

Fig. 1. Experimental Arrangement.

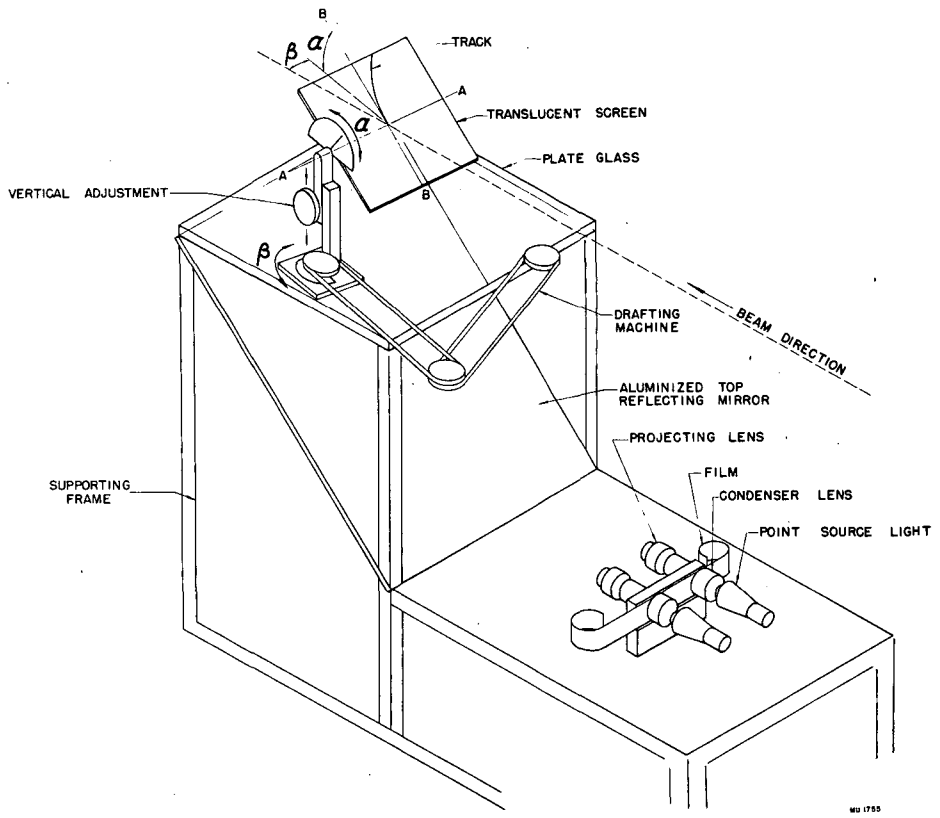

Fig. 2. Schematic Drawing of Stereoscopic Projector.
This figure, taken from Reference 4, shows an earlier model than the one actually used in this experiment.

be hidden by such an arrangement, the plate was rotated for the second run so that the mesons entered the plate at about 30° from the normal. The 7.33-kilogauss field was used in this second run.

Photography

Pictures were taken with a stereoscopic camera placed 27.5 inches above the cloud chamber. The 5-cm Leitz Summitar lenses were operated between f/8 and f/11. The light flash was furnished by two General Electric FT-22 tubes, and was initiated by means of a tickler coil; the tubes then discharged 250-microfarad condensers charged to 1.5 kilovolts. The film used for this experiment was 1.80-inch Kodak Linagraph. The film was processed continuously by means of an automatic developer attached to the camera. The negative could be viewed ten minutes after the photograph was taken.

Reprojection

The negatives were analyzed by means of a stereoscopic reprojection system[4] which closely reproduced the optical conditions prevailing when the photographs were taken. The main features of the apparatus are shown in Fig. 2. Light from K-300 Sylvania Concentrated Arc lamps passes through the films and reprojects the two images on a translucent screen. Because the tracks are very nearly plane curves, the two images of a track coincide only if the screen lies in a plane that corresponds to the plane of the original track in the cloud chamber. After the coincidence has been achieved, the screen is rotated until two perpendicular reference lines inscribed on it lie along the tangent and normal of the curve. The two spherical coordinate angles α and β are then indicated on appropriate scales. The radius of curvature is measured by matching arcs inscribed on lucite templates to the curve. For events occurring in the plate the tracks are extrapolated to the center of the plate. The exact position in the chamber is also recorded.

The information was transcribed to Keysort cards. Use of these cards greatly simplified the handling of the data.

III. REDUCTION OF DATA

A. Scanning Procedure

All pictures were scanned on the reprojection apparatus described. For this purpose the glass screen was kept in a horizontal position and only one view was projected on it. All incoming meson tracks were followed to the plate and those satisfying certain criteria were counted as flux particles. These criteria are described in the next section. Events other than small-angle scatters were noted and investigated, both images being used for space reprojection.

All pictures were also independently scanned for events by the more rapid method of using a stereoscopic viewer. Many events could not be identified with certainty by this method because the image is smaller and actual measurements cannot be made. Usually these doubtful events were easily resolved by the reprojector analysis. This viewer scanning, therefore, was used only as a check on the efficiency of the reprojector method in finding events. Only one stop was found in the viewer scanning that was not noted in the reprojector method.

B. Meson Flux

To be able to calculate absolute cross sections, one must know the actual meson flux. For that reason pictures were scanned not only for events but also for the number of acceptable mesons.

Acceptance Criteria

To obtain detailed information about the meson flux, all the meson tracks in a series of pictures were measured. From these measurements was derived a set of acceptance criteria.

The mean values of the angles α and β for entering mesons were determined as a function of position along the plate. Mesons within angular intervals of $\delta\alpha = \pm 3.5^{\circ}$ and $\delta\beta = \pm 4^{\circ}$ were accepted for the 5.18-kilogauss field data; intervals of $\delta\alpha = \pm 4^{\circ}$ and $\delta\beta = \pm 5^{\circ}$ were used for the 7.33-kilogauss field data.

The height of the tracks was restricted to a region 2.3 inches high in order to insure good visibility of both the entering and emergent tracks, and to be certain that the meson passed through the lead plate.

The radius of curvature ρ was required to be between 67 and 98 cm for the low-field data and between 47 and 69 cm for the high-field data, corresponding to an energy region of 35 to 65 Mev.

Flux Counting

The scanner followed each entering meson track to the plate and checked the β and ρ criteria by means of a template containing the limiting radii of curvature and the angular limits of β. If a track appeared to be faint or to fade near the plate, its height and dip angle were measured; such tracks generally did not satisfy the acceptance criteria.

The flux count from the reprojector scanning for the entire experiment is listed below. Also listed are the numbers of mesons in a series of pictures for which the reprojector flux count was checked by actual measurement of each track. Because the reprojector flux count is estimated to be accurate to about 5%, the agreement between these numbers is satisfactory.

	Low Field	High Field
Total Flux (Reprojector Scanning)	22,022	6,550
Flux Sample (Reprojector Scanning)	433	151
Flux Sample (Detailed Measurement)	419	157

Beam Contamination

The meson flux had still to be corrected for positron and μ-meson contamination, since the tracks of these particles with the same magnetic rigidity as 50-Mev π-mesons could not be distinguished from the tracks of the π-mesons, for the following reason: The ionization of a 50-Mev π^+-meson relative to minimum ionization is 1.52; that of a μ-meson with the same curvature (momentum) is 1.03; of a positron it is 1.59. Such small variations in ionization would not be noticeable in this experiment, as the mesons arrived in pulses spaced 1/60 second apart and the difference in droplet age is sufficient to mask these ionization variations.

Positrons. High-energy positrons passing through a 1/8-inch lead plate are likely to lose a large fraction of their energy. Events of this kind were noted in the scanning. The number of such events was divided by the theoretical probability of their occurrence to obtain the total flux of positrons. It was found that about 0.5% of the incident

tracks were due to positrons. Details are given in Appendix I.

μ-Mesons. The μ-meson contamination was calculated by considering the decay rate of the π-mesons, the angular and energy distributions of the resulting μ-mesons, and the geometric arrangement of the collimators. The μ-meson contamination was thereby estimated to be 11%. The details are given in Appendix II.

Corrected Flux

The meson flux corrected for positron and μ-meson contamination is listed below. Also listed is the actual amount of lead traversed, which is proportional to the secant of the mean angle between the meson flux and the normal to the plate.

The total amount of lead traversed is 8.69×10^4 g/cm^2 and is estimated to be accurate to 5%.

Field (kilogauss)	Corrected Flux	Mean Angle (degrees)	Path in Lead (g/cm^2)
5.18	1.95×10^4	5	6.53×10^4
7.33	1.69×10^3	15	5.84×10^3
7.33	4.10×10^3	30	1.58×10^4

C. Elastic Scatters

All scatters with projected deflections greater than 30°, as seen on the horizontal screen, were investigated in detail. These data were used to calculate the angular distribution of scatters greater than 40°. A sample corresponding to a flux of 6,576 tracks was examined for scatters with projected deflections greater than 20° and was used for the angular distribution between 25° and 40°. A sample of 209 tracks was used for the smaller-angle scattering.

Scattering Formulas

The scattering angle θ is calculated from the angles α and β of the incident track (i) and scattered track (s) by using the formula

$$\cos\theta = \cos\alpha_i \cos\alpha_s + \sin\alpha_i \sin\alpha_s \cos(\beta_i - \beta_s). \quad (1)$$

For angles smaller than 30° the following approximation was used,

$$\theta^2 = (\alpha_i - \alpha_s)^2 + (\beta_i - \beta_s)^2, \quad (2)$$

and for backscatters greater than 150°,

$$(180 - \theta)^2 = (\alpha_i + \alpha_s - 180)^2 + (\beta_i - \beta_s + 180)^2. \quad (3)$$

Corrections

When the projected deflection is limited to a minimum value β_o, a correction factor $f(\theta)$ must be applied to the number of scatters observed, in order to compensate for the scatters with a scattering angle θ but having a projected deflection $|\beta_i - \beta_s| \leq \beta_o$. Since the α_i of the incident meson was very close to 90°, this correction factor is simply

$$f = \frac{90}{\phi},$$

where ϕ is the angle (in degrees) given by

$$\cos\phi = \tan\beta_o \cot\theta. \qquad (4)$$

The geometric relationships are illustrated in Fig. 3.

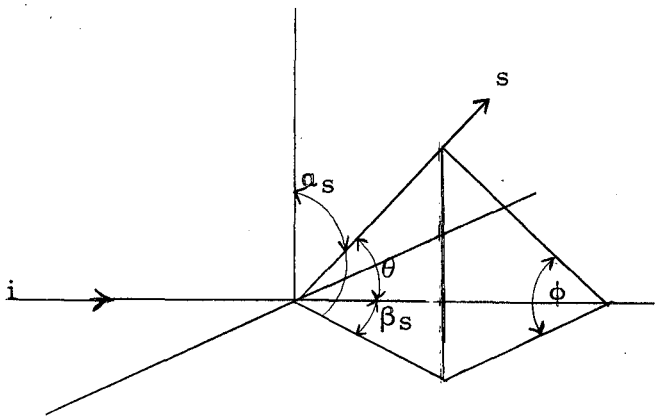

Fig. 3

For scatters near 90° two other corrections must be applied. One of these compensates for the loss of scatters at steep angles; the other takes account of the mesons scattered into the lead plate and stopped within the plate.

The limitation of the steepness of the scattered track to $\alpha_s \leq \alpha_o$ requires a correction factor $f(\theta)$ as above, with the ϕ now given by

$$\sin\phi = \cos\alpha_o \csc\theta. \qquad (5)$$

The value of α_o used was 30°.

For the major portion of this experiment the mesons entered very nearly normal to the plate. Thus many scatters near 90° would not be observed. An appropriate correction factor was calculated and used; it was 2.70 for the 80°-to-90° and 90°-to-100° intervals, and 1.04 for the 70°-to-80° and 100°-to-110° intervals. The calculations are outlined in Appendix III. Also, sufficient data were obtained with mesons impinging on the plate at about 30° to show that no unusual features occurred in the 80°-to-110° interval.

Azimuthal Distribution

The azimuthal distribution was checked for the accepted scatters with scatter angles greater than 40°. The events were first assigned to quadrants according to the signs of $(\alpha_i - \alpha_s)$ and $(\beta_i - \beta_s)$, or their counterparts in Eq. (3) in the case of backscatters. The numbers per quadrant were 12.5, 12, 11.5, 15; the two halves belong to a borderline case. In view of the smallness of the samples the agreement is satisfactory.

The data of all four quadrants were then combined to yield the azimuthal distribution as a function of scatter angle. This is shown in Fig. 4. The azimuthal angle ϕ is given by $\tan\phi = \tan|\alpha_i - \alpha_s| \csc|\beta_i - \beta_s|$, or its counterpart in the case of backscatters. The limits imposed by the acceptance requirements of α_o and β_o are indicated. Four events are also shown which were excluded on the basis of these limits. Again, the distribution is reasonably uniform in ϕ.

D. Inelastic Scatters

All flux mesons passing through the lead plate lose about 5 Mev. The consequent small increase in ionization (10%) and decrease of curvature (4%) was not apparent to the scanner. Twelve events were found that could be inelastic scatters with energy loss of more than 50%, but only one event was actually given this interpretation, the remainder being classed as π-μ decays or as proton events.

Meson Decays Resembling Inelastic Scatters.

π-μ decays within the lead plate or in the masked region in front of the plate may have the same appearance as inelastic scatters. Seeming inelastic scatters were identified as π-μ decays if the energy-angle relationship of the tracks (extrapolated to the center of the lead plate) satisfied the calculated π-μ correlation. Eight of the observed events were thus classed as π-μ decays. The expected number of π-μ decays within the 1/8-inch lead plate was 12.3, half of them having considerably decreased curvatures. If the invisible region in front of the plate is taken to be 1/16 inch, then the resulting total number of expected π-μ decays resembling inelastic scatters is nine.

Proton Events

In three of the events, the emergent tracks were very steep and heavily ionizing. They appeared to be proton tracks and were classed

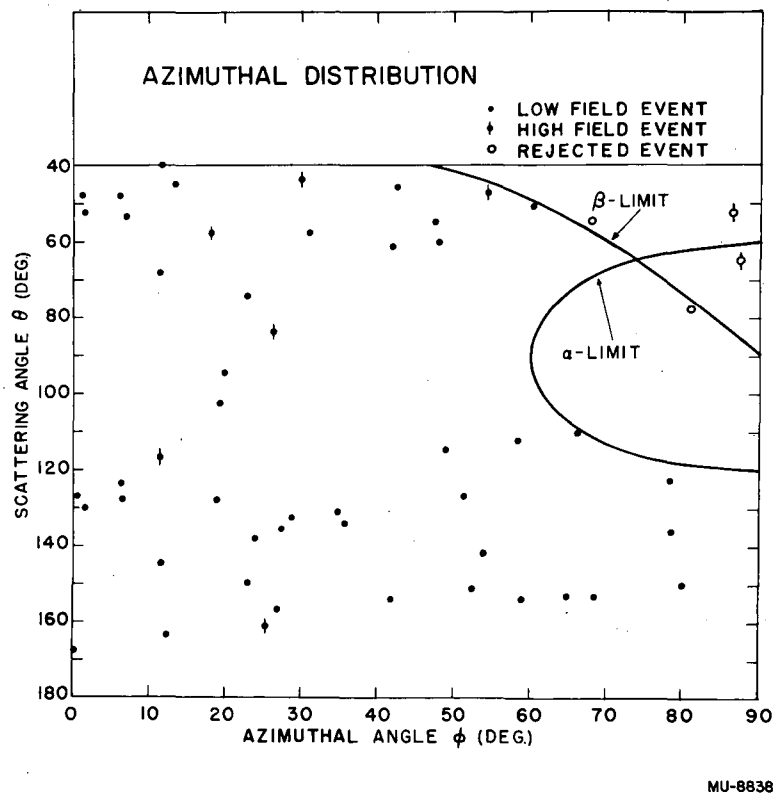
AZIMUTHAL DISTRIBUTION
LOW FIELD EVENT
HIGH FIELD EVENT
REJECTED EVENT
β-LIMIT
α-LIMIT
SCATTERING ANGLE θ (DEG)
AZIMUTHAL ANGLE φ (DEG.)
40
60
80
100
120
140
160
180
0
10
20
30
40
50
60
70
80
90
MU-8838

Fig. 4

as such, but because no curvature measurement was possible this identification was not entirely certain.

E. Charge-Exchange Scatters

Characteristics of Events

In a charge-exchange scatter the π^+-meson is changed into a π^0-meson, which in turn disintegrates into two photons. The latter process occurs within a few microns of the actual scatter, thus both can be considered to occur at the same point in the lead plate. There is a 28.5% likelihood[5] that one of the two photons may create a positron-electron pair in the lead plate, and a 1.45% likelihood[6] of the π^0-meson's decaying directly into an electron pair and a photon.

A charge-exchange scatter was therefore required to consist of a π-meson stop and a high-energy pair emerging from the same point in the lead plate.

Apparent Charge-Exchange Scatters

High-energy positrons passing through the lead may radiate photons which in turn may produce a positron-electron pair. Such an event would look much like a true charge-exchange scatter. Since the bremsstrahlung spectrum from the electrons is strongly peaked in the forward direction, these events were excluded by requiring the angle between the incident track and the pair to be at least 20°.

The fraction of charge-exchange photons emerging into the $0^\circ - 30^\circ$ interval was expected to be only 2%. This estimate was based on an angular distribution of π^0-mesons, which was taken to be the same as that measured[7] for the process $\pi^- + p \rightarrow \pi^0 + n$. The photon angular distribution with respect to the π^0-meson was calculated from the π^0 decay kinematics, and was folded into the π^0 angular distribution to obtain the photon angular distribution in the laboratory system. The distribution also indicates that 70% of the photons emerge into the backward hemisphere.

Correction Factor

When the conversion efficiency for the photons and the frequency of the alternate mode of π^0 decay are combined, they yield a value of 29.6% likelihood of a charge-exchange scatter's being identifiable in the present experiment.

More elaborate calculations were not carried out because only two events were found that satisfied the requirements of charge-

exchange scatters. Besides these events in which the pairs were in the backward hemisphere, seven apparently electron-induced pairs were found with the angles of emergence less than 15°, and one at 19°.

F. Proton Events

In a proton event the meson stops in the lead and one or more protons emerge from the same point. Usually this type of event is easily identifiable because the proton track curvature is larger and its ionization is noticeably heavier than meson tracks.

Proton Energy

The proton energy was determined from the curvature and also from the ionization. In most cases the two values agreed within the estimated accuracies. In cases of doubt, more weight was given to the ionization estimate, as the turbulence sometimes made curvature measurements quite unreliable. The proton energies so determined are probably accurate to 40%.

Uncertain Events

In a few instances the heavy prongs could not be unambiguously identified as protons. In three cases (two of them occurring in the high field) the heavy tracks might have been due to inelastically scattered mesons, and in two cases they might have been due to deuterons.

G. Stops

Those events in which a meson track ended in the lead and in which no track originated from the same point were classified as stops.

Interpretation

Stops may actually be large-angle scatters, charge-exchange scatters, stopped electrons, inelastic scatters, or stars with no visible prong emerging from the lead. The numbers of stops due to the first three of these possibilities were calculated as indicated in the preceding sections to be 2.04, 4.76, and 0.97 respectively. Inelastic scatters were not considered. All the remaining stops were interpreted as stars with no detectable prongs, or true stops.

H. Acceptance Criteria for Events

In Section III B acceptance criteria for flux mesons were described. The same criteria were also applied to event-inducing mesons, and only events induced by flux mesons were used in the calculations.

IV. RESULTS AND DISCUSSION

The most important cross sections are listed below in Table I. The uncertainties listed include the 5% uncertainty in the meson flux and the standard deviation of the number of events observed. The actual number of events observed is given in parentheses. The results of this experiment are discussed and compared with results from related experiments in the following sections.

Table I

Cross Sections in Millibarns

Elastic Scatters >40°	Stops	1-Prong Stars	2-Prong Stars	Charge Exchange	Total Inelastic Events*	Total
252±36	591±56	234±33	28±10	27±19	883±73	1136±89
(51)	(157)	(59)	(7)	(2)	(226)	(277)

* This includes the one observed inelastic scatter.

A. Elastic Scattering

Angular Distribution

The angular distribution of the elastically scattered mesons is shown in Fig. 5. At small angles multiple Coulomb scattering predominates. The root-mean-square scatter angle was measured to be 11°. This agrees with the theoretical value obtained from a formula given by Rossi and Greisen.[8]

The main features of this angular distribution, namely the minimum near 90° and the large amount of backscattering, have been noted in all other meson scattering experiments by complex nuclei below 100 Mev. These experiments include the elements He,[9] Li,[10] Be,[11] C,[12, 13] and Al,[1, 10] investigated by cloud chamber techniques[1,9,11, 12] and counters,[10, 13] as well as experiments of scattering in nuclear emulsions.[14-17] Above 100 Mev the angular distribution is more nearly isotropic, as shown by experiments in He,[9] Li,[10] C,[18] Al,[10] and Pb.[18]

Comparison of Backscattering Cross Section

The large-angle scattering of 33-Mev π^--mesons in Al, Cu, and Pb has been investigated by Heckman and Bailey.[19] The backscattering cross section for lead was found to be 577±80 mb. The backscattering

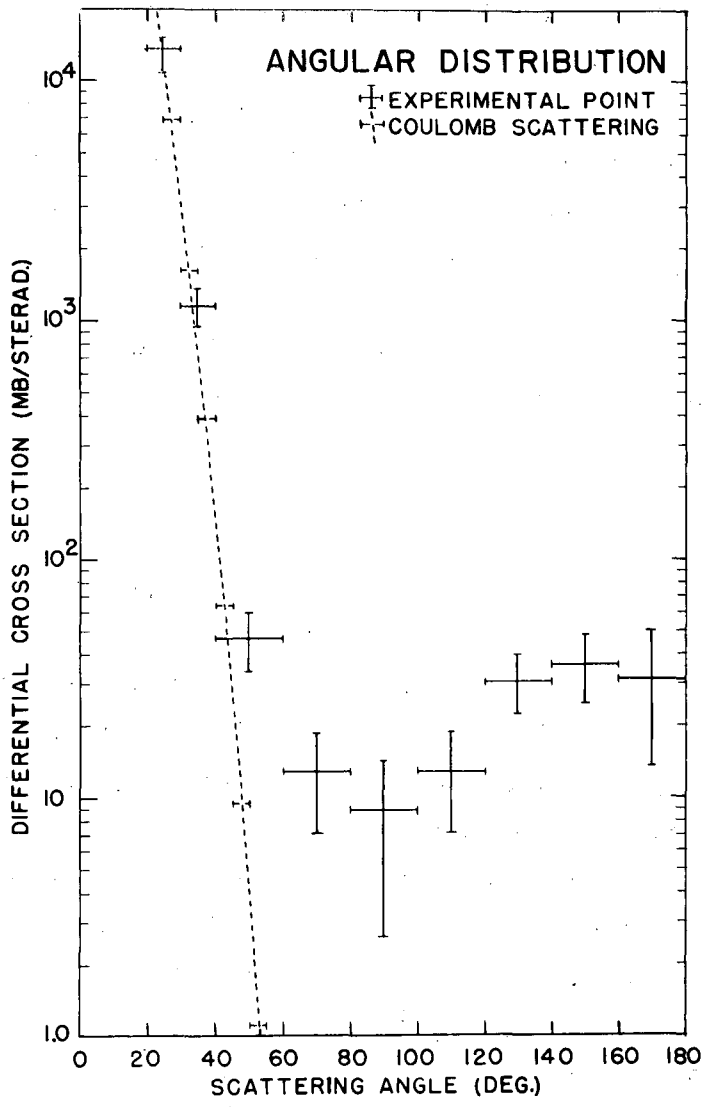
ANGULAR DISTRIBUTION
EXPERIMENTAL POINT
COULOMB SCATTERING
DIFFERENTIAL CROSS SECTION (MB/STERAD.)
10^4
10^3
10^2
10
1.0
0
20
40
60
80
100
120
140
160
180
SCATTERING ANGLE (DEG.)

MU-8748

Fig. 5

cross section for 50-Mev π^+-mesons in lead found in this experiment is 143±26 mb. The cross-section ratio of 4.0±0.9 may be explained largely in terms of two factors:

1. The Coulomb effect reduces the effective area of the nucleus for positive mesons and enhances the cross section for negative mesons. A consideration of the impact parameter yields the approximate Coulomb factor for positive mesons,

$$f^+ = 1-(V_c/T). \qquad (6)$$

V_c is the Coulomb energy given approximately by $ZA^{-1/3}$(in Mev) and T is the kinetic energy of the mesons. This Coulomb factor is 0.72 for 50-Mev π^+-mesons in lead and 1.42 for 33-Mev π^--mesons. The ratio of the Coulomb factors is 1.97 : 1.

2. Elastic meson-nucleon backscattering is almost entirely due to $\pi^+ + p$ (or $\pi^- + n$) scattering.[20, 21] Hence, the neutron-proton ratio in lead may well have a bearing on the relative backscattering cross sections of mesons of different sign. For lead the neutron-proton ratio is 1.52 : 1. Combining this ratio with the Coulomb factors produces a 3.0 : 1 ratio, which is to be compared with the observed (4.0 ± 0.9) : 1 ratio.

Thus these two factors can largely account for the cross-section ratio. Some weight is lent to such a free-nucleon model by the results of Heckman,[19] which indicate that backscattering cross sections at this energy are proportional to the atomic number and are consistent with energy independence in the case of lead. However, further data are still needed to clarify the applicability of such a model.

Fig. 10 in Appendix IV shows an example of an elastic backscatter.

B. Inelastic Scattering

Only one event was identified as an inelastically scattered flux meson. The cross section corresponding to one event is 4.0 mb. Two other inelastic scatters were observed, but the incident mesons did not satisfy the acceptance criteria because of their high energy. The energies and scatter angles of the three events are listed below.

Initial Energy (Mev)	Final Energy (Mev)	Scatter Angle
43	6.5	46°
76	44	175.5°
98	2	29°

A picture of the last of these events is shown in Appendix IV (Fig. 11).

A small value of the cross section for inelastically scattered 50-Mev π^+-mesons is not unexpected. Previous meson scattering experiments have indicated that the inelastic-scattering cross section for positive mesons below 50 Mev is very small. Only two detectably inelastic scatters were found by Bernardini and Levy[22] in 3, 120 cm of track length in emulsions; in a similar experiment by Rankin and Bradner[17] not a single inelastic scatter was found in 902 cm of track length; and in a cloud chamber experiment by Tenney and Tinlot[11] using beryllium for a scatterer no inelastic scatters were detected.

Above 60 Mev the inelastic-scattering cross section of π^+-mesons rises rapidly with energy, as shown by the nuclear plate data of Minguzzi, Puppi, and Ranzi,[14] and Bernardini and Levy,[22] and by the cloud chamber work of Byfield, Kessler, and Lederman[12] with carbon. The occurrence in this experiment of two inelastic scatters among the relatively few high-energy mesons is in qualitative agreement with a rapid energy dependence of this process.

C. Charge-Exchange Scattering

Description of Observed Events

Besides the two accepted charge-exchange scatters, one other event was seen that was induced by a meson of energy higher than 65 Mev. The energies and angles of the events are listed below. Also included is the event where the angle was 19° and which was interpreted as being due to a positron. The last three events are reproduced in Figs. 12-14 of Appendix IV.

Incident Energy (Mev)	Pair Energy (Mev)	Angle Between Meson and Pair
61	63.5	161°
65	64	136°
72	40.5	40.5°
111-Mev positron (39 Mev if π^+-meson)	60.5	19°

Summary of Previous Experiments

Charge-exchange scattering of π^--mesons in hydrogen has been investigated at several energies.[7, 20, 21, 23, 24] At present the work with heavier elements is still incomplete. At 34 Mev the cross

section for exchange scattering in deuterium[23] is the same for mesons of either sign, in agreement with predictions from charge symmetry. Near 40 Mev the cross section in deuterium as well as in some other light elements [23, 25] seems to be considerably smaller than the hydrogen cross section. At 60 Mev and 105 Mev, however, the exchange scattering cross section in helium[9] appears to be considerably larger than in hydrogen. At 125 Mev the charge-exchange cross sections for π^--mesons in carbon and lead[18] are respectively 20^{+20}_{-10} and 100^{+80}_{-40} millibarns.

In view of the fact that only two events were observed in this experiment, the value of 26.8 ± 19 mb for the charge-exchange scattering cross section is rather uncertain.

D. Absorption Cross Section

Comparison with Previous Experiments

Transmission experiments[26-30] have shown that for complex nuclei the total cross sections increase with increase in energy, reaching geometric values near 85 Mev and showing no evident energy dependence thereafter. These cross sections include the inelastic processes as well as the large-angle scatters.

The total cross section of 37-Mev π^+-mesons in lead has been measured by Button.[28] This measurement includes scatters greater than 70° but has not been corrected for fast star prongs. The latter effect may increase the measured cross section of 1300 ± 70 mb by as much as 15%. The corresponding cross section of inelastic processes and scatters greater than 70° as measured in this experiment is 1044 ± 83 mb. The ratio of the cross sections is 1.24 ± 0.12, but if the Coulomb effect of Eq. (6) is applied, this ratio is increased to 1.44 ± 0.14. The agreement between these measurements is poor, particularly because the cross section would be expected to increase with energy. However, there seems to be no obvious explanation for such a large systematic error in this experiment.

Mean Free Path

The absorption cross section may be used to calculate the mean free path of π-mesons in nuclear matter. The optical model[31] furnishes a relation between the cross section for incoherent processes and the mean free path. The incoherent processes of this experiment include

the inelastic processes of true absorption, charge-exchange and inelastic scattering. It is a question of interpretation whether the large-angle elastic scatters are coherent or incoherent. If all elastic scatters are considered to be coherent (diffraction) scatters, then the mean free path is $(12.4 \pm 1.7)\,10^{-13}$cm. If, however, the elastic scatters greater than 70° are interpreted as incoherent scatters and are included in the incoherent cross section, the mean free path is found to be $(9.0 \pm 1.5)10^{-13}$cm. The interpretation of the large-angle scatters as meson-nucleon scatters and therefore as incoherent scatters, would be consistent with the features of backscattering noted in Section IV A. However, more information is still needed to clarify the validity of such an interpretation.

The variation with energy of the mean free path of π-mesons in nuclear matter has been investigated by Stork.[30] Stork analyzed his own data for copper and lighter elements, as well as the data from other workers for inelastic processes in carbon and emulsions by means of the optical model, and fitted the mean free paths obtained in this way to an E^2/p^4 energy dependence. E is the total relativistic meson energy and p is the meson momentum. The resultant curve with a least-squares fit indicates a value of $(7.1 \pm 0.6)10^{-13}$cm for the mean free path at 50 Mev. The discrepancy between this value and the one obtained in the experiment reported here may be due in part to the approximate value of the Coulomb factor used and possibly also to a difference between the absorption mechanism in lead and that in the lighter elements.

E. Analysis of Star Fragments

The characteristics of the star fragments from meson-induced stars are of interest because they may reflect the mechanism of the meson absorption process in complex nuclei. Although the use of a 1/8-inch lead plate in this experiment seriously limited the number of observable fragments, the results may nevertheless be of interest. The results are listed below, and are compared to predictions from two models of meson absorption. Examples of proton events are shown in Figs. 14, 15, and 16 of Appendix IV.

Results

Figure 6 is a plot, for all proton events, of the proton energy versus the angle between the proton and the incident meson. This figure must be interpreted with due consideration of the orientation of the lead

plate. For example, 70-Mev protons produced within the lead and emerging normal to the plate ($\theta \approx 0^{\circ}$) lose as much as 16 Mev; at 68° such protons begin to be attenuated; the mean energy of the emergent protons is 55 Mev. Protons of 40 Mev initial energy begin to be attenuated at 15°; at greater angles half of the emergent protons have energies of less than 20 Mev.

Table II lists the observed protons in 60° intervals. Also listed are the percentages of protons that would emerge into these intervals if protons were produced uniformly throughout the lead and ejected with spherical angular distributions. The initial proton energy is taken at 70 Mev and also at 40 Mev.

Figure 7 is a plot, for all two-prong events, of the total prong energy versus the angle between the prongs. Included in this figure are a few events induced by mesons that did not satisfy all the criteria required of acceptable flux mesons.

Two-Nucleon Absorption Model

The simplest mechanism[32, 33] of meson absorption requires the participation of two nucleons in order to conserve momentum and energy. In the center of mass of the two-nucleon-meson system, each of the nucleons receives half of the total meson energy. The frequent appearance of two high-energy protons emerging in nearly opposite directions from π^+-meson-induced stars[1, 11, 12, 34] is evidence for the occurrence of the process $\pi^+ + d \rightarrow 2p$. Only one prong would be visible in the case of $\pi^+ + 2n \rightarrow p + n$.

As indicated in Fig. 7, the few two-proton events observed in this experiment show a preference for a large angle between the prongs; in all these events, however, one proton has less than 20 Mev energy. This lack of two-prong events with proton energies near 90 Mev may be explained by collisions of the nucleons inside the lead nucleus. To estimate this effect, the lead nucleus was assumed to be a uniformly dense sphere of radius 8.3×10^{-13} cm, and a mean free path of the nucleons of 3.3×10^{-13} cm was used.[31, 35] The probability of escape, without collision, of a randomly produced nucleon was calculated to be 28%. The probability of escape of two nucleons without collision is only 1% if the initial angle between them is 180°. Only half of this 1% will have the prongs in the unobstructed forward and backward

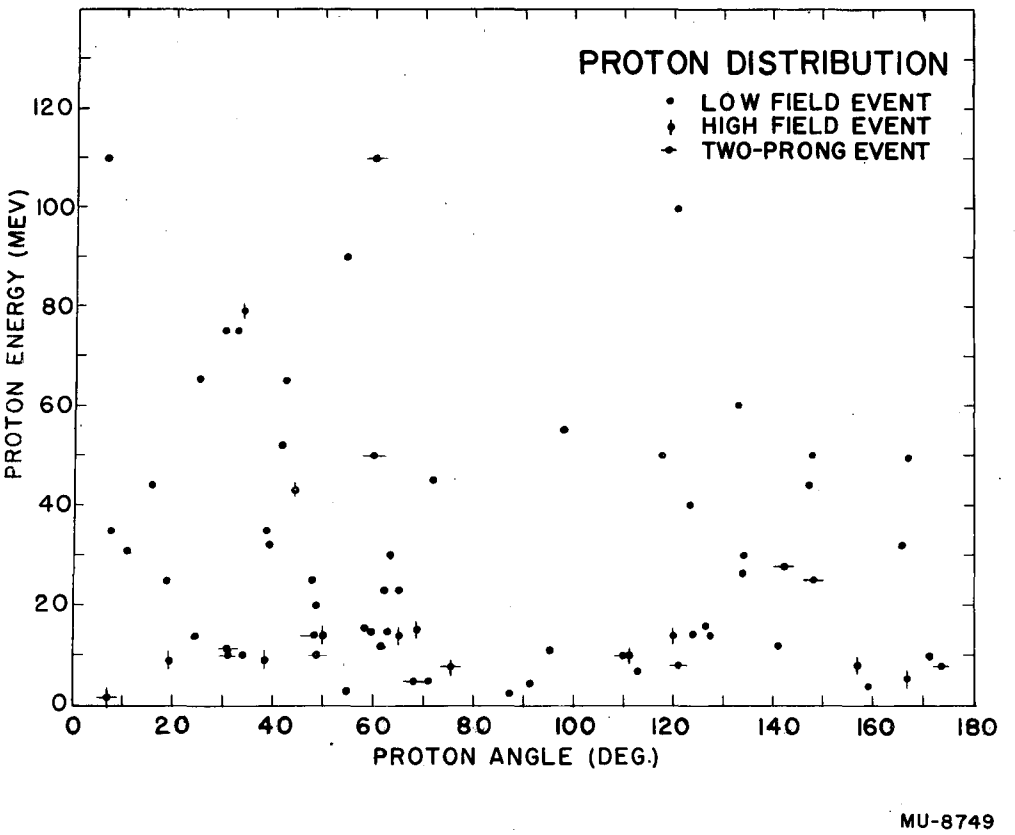
PROTON DISTRIBUTION
LOW FIELD EVENT
HIGH FIELD EVENT
TWO-PRONG EVENT
PROTON ENERGY (MEV)
0
20
40
60
80
100
120
PROTON ANGLE (DEG.)
0
20
40
60
80
100
120
140
160
180
MU-8749

Fig. 6

Table II

Proton Angular Distribution

	Angular Interval 0-60°	61°-119°	120°-180°	Total
Number of Observed protons				
≥ 20 Mev	19	6	11	36
< 20 Mev	13	13	11	37
Theoretical Percentage of Emergent Protons				
70 Mev	26	39	26	91
40 Mev	19	16	19	54

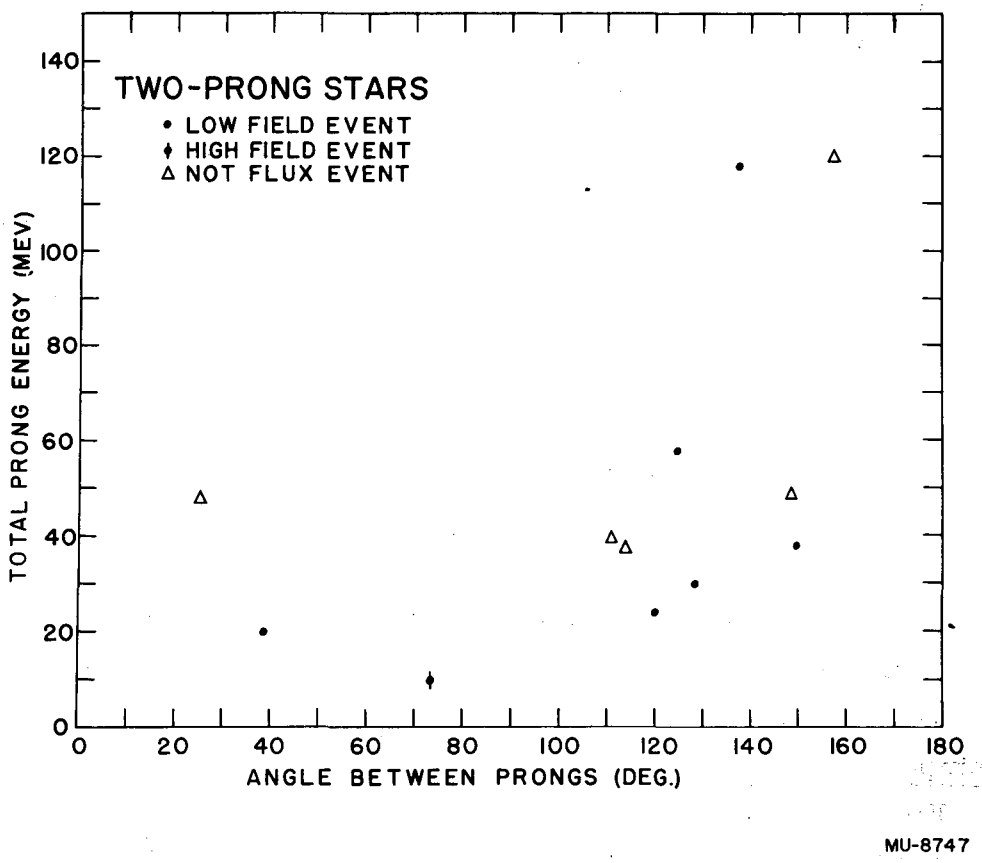
TWO-PRONG STARS
• LOW FIELD EVENT
ϕ HIGH FIELD EVENT
Δ NOT FLUX EVENT
TOTAL PRONG ENERGY (MEV)
ANGLE BETWEEN PRONGS (DEG.)
0
20
40
60
80
100
120
140
160
180
MU-8747

Fig. 7

60° cones, and only about half again will be (2p) rather than (n+p) events. For the total of 215 stars (true stops and proton events) of this experiment only 0.5 observable two-prong events with opposite prongs can be expected. The two-prong events of this experiment are, however, in qualitative agreement with the occurrence of a two-nucleon absorption process which is followed by collisions of the nucleons within the lead nucleus. The nucleons are thereby degraded in energy and the angle between them is generally decreased; but the predominantly opposite directions of the two nucleons are preserved to a large extent as indicated by the 9:3 ratio of the events with angles greater than 90° to those with angles less than 90°.

Many-Nucleon Absorption Model

Careful experiments[36-38] with stars produced by slow π^--mesons in nuclear emulsions indicate that usually more than two nucleons take part in the primary absorption process. Evidence for the occurrence of such a process rests on the occasional appearance of star prongs with a large fraction of the total meson energy. Such prongs have also been found in stars produced by fast mesons. It has been estimated[11, 34] that for fast mesons the multinucleon process occurs in approximately one-third of the absorptions, while the other absorptions proceed via the two-nucleon process.

In this experiment only three protons above 100 Mev were found. These energies are estimated to be accurate to 40%, and if the upper limits are assumed to apply, these events could be interpreted in terms of a multinucleon absorption process.

Comparison of Models

For the data of this experiment, the relative importance of the two models may best be estimated by considering the asymmetry in the angular distribution of the protons. The momentum of the 50-Mev meson will be more effective in producing forward-to-backward asymmetry of the protons in the mechanism involving fewer nucleons. If the nucleons are assumed to be at rest in the laboratory system and to scatter with spherical symmetry in the center-of-mass system then the ratio of nucleons in the 60° forward cone to those in the 60° backward cone is 1.59 for the two-nucleon case, as compared to 1.21 for a four-nucleon case (e.g. an α-particle). Use of a

$0.2 + \cos^2\theta$ angular distribution in the center-of-mass systém as observed by Durbin et al[39] for the process $\pi^+ + d \rightarrow p + p$, results in ratios of 1.31 and 1.11 respectively.

Figure 6 and Table II show that in this experiment the ratio of emergent fast protons in the 60° forward cone to those in the 60° backward cone is 19:13 for protons of at least 20 Mev, and 10:4 for protons of at least 50 Mev, thus favoring a two-nucleon model of meson absorption.

The low-energy protons show a nearly even distribution. These low-energy protons are interpreted as resulting in part from a boil-off process following the primary act of meson absorption, and partly from collisions of the primary nucleons within the nucleus, and are therefore expected to show only a slight forward asymmetry.

Similar results have been obtained in a number of previous experiments. In a study by Blau et al,[34] of stars induced by 50-to 80-Mev π^+-mesons in nuclear emulsions, the fast prongs corresponding to protons of more than 30 Mev display a rather wide angular distribution. Some asymmetry is shown, however, in the forward-to-backward ratio which, for fast prongs in emulsion stars, is 26:14. This is in good agreement with the 53:29 ratio previously obtained by Bernardini and Levy.[22] The angular distribution of the slow prongs is nearly isotropic.

For meson scattering in beryllium[11] the ratio of the fast protons in the forward 60° cone to those in the backward 60° interval was found to be 2.7 ± 1.0. One conflicting set of ratios was found in aluminum,[1] however, where no apparent forward-to-backward anisotropy existed for fast protons, their ratio being 24:25, while the slow protons exhibited a 25:9 forward-to-backward asymmetry.

F. Energy Dependence

In this experiment the number of events at various energies was insufficient to permit one to draw any conclusions about the energy dependence of the cross sections. The data are given in Fig. 8, which shows the number of events plotted versus meson energy and also the flux spectra corresponding to the flux samples mentioned in Section III B.

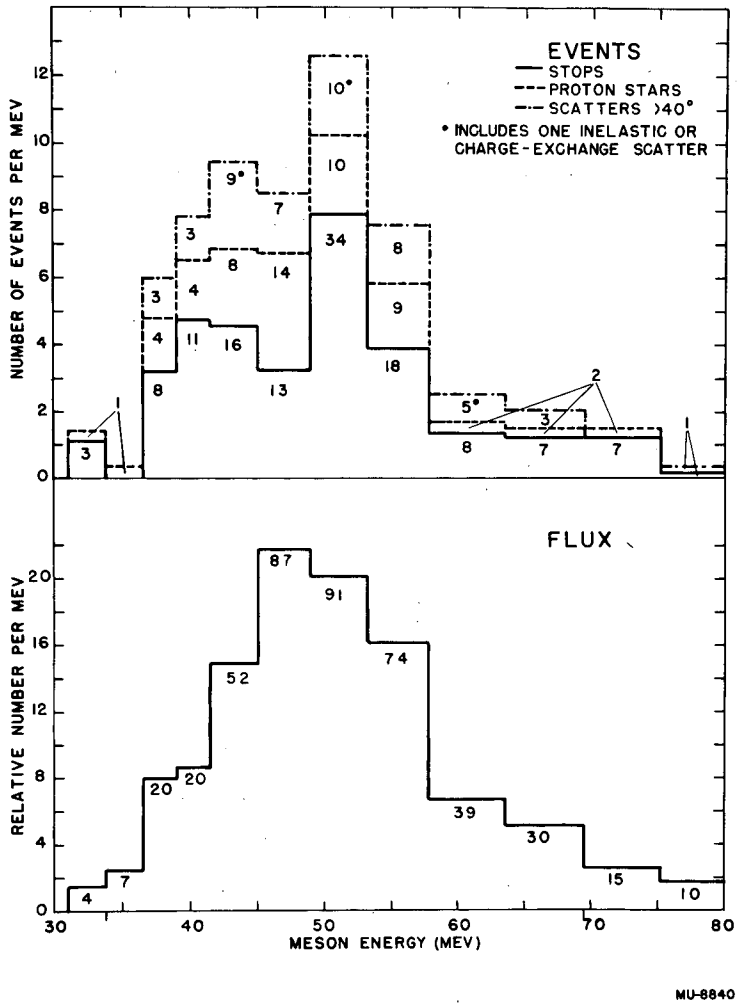

Fig. 8a. Energy Dependence of Events.
Data for 5.18-Kilogauss Field.

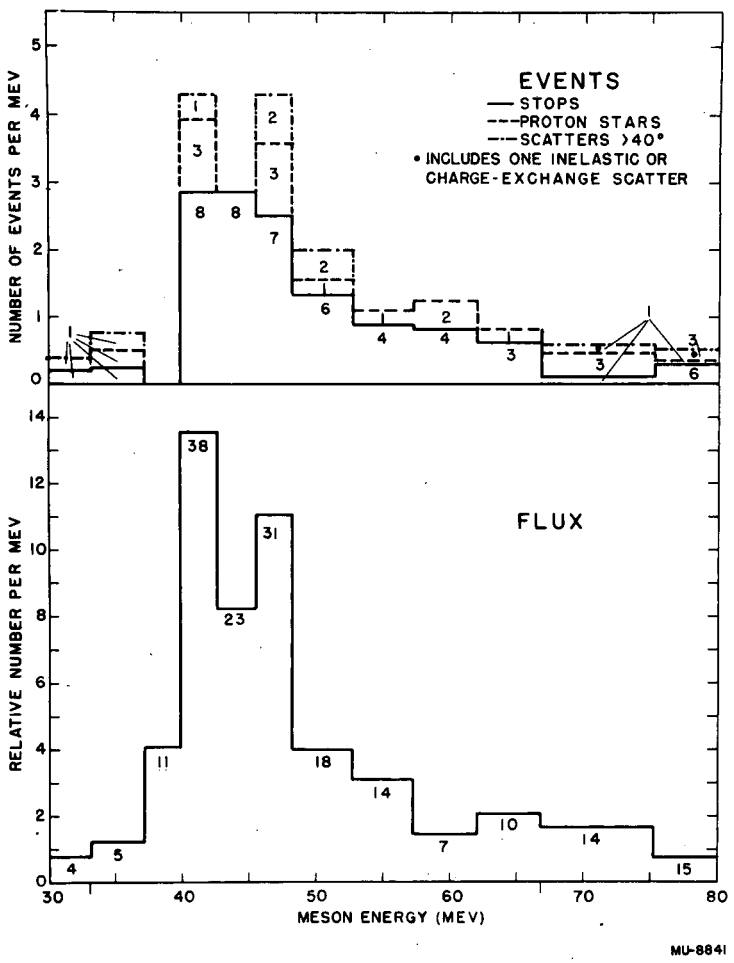

Fig. 8b. Energy Dependence of Events.
Data for 7.33-Kilogauss Field.

V. SUMMARY

The main results of this experiment are as follows:

1. The total cross section of 50-Mev π^+-mesons in lead is 1136±89 mb.

2. The angular distribution for elastic scattering has a minimum near 90°.

3. The ratio of elastic to inelastic processes is 1:(4.5±0.7).

4. Charge-exchange scattering constitutes about 3% of the inelastic cross section, and inelastic scattering constitutes about 0.5%.

5. The star-fragment distribution is not inconsistent with an absorption process involving only two nucleons.

ACKNOWLEDGMENTS

The advice, encouragement, and helpful contributions of Professor Wilson M. Powell are gratefully acknowledged. The writer also benefited from the earlier work of Dr. James Tracy. Thanks are also due to the other members of the cloud chamber group, particularly Messrs. John Elliott, Larry Oswald, and Howard White, and Miss Barbara Schultz, as well as to the cyclotron staff. This work was performed under the auspices of the U. S. Atomic Energy Commission.

APPENDIX I

Positron Contamination

Theoretical Spectrum

The probability that an electron, having passed through the lead plate, would emerge with a fraction ϵ of its initial energy was calculated by means of a formula given by Heitler.[5] For a 1/8-inch lead plate this probability can be expressed as $W(\epsilon)d\epsilon = 0.80\ (\ln 1/\epsilon)^{-0.27} d\epsilon$.

Comparison with Experiment

Because all particles passing through the lead plate lose energy, the scanner only recorded events in which the curvature or ionization changed markedly. Positron events in which the energy decreased by more than 40% were certain to be recorded and were therefore used for the comparison of the experimental spectrum with the theoretical one.

Positron Flux

An upper limit of the positron flux was obtained by matching the experimental spectrum with $\epsilon \leqslant 0.6$ to the theoretical spectrum. Figure 9 shows this comparison for positrons having the same curvature as 50±7-Mev π^+-mesons. The 34 events constitute 45.2% of the theoretical spectrum. The entire spectrum therefore corresponds to 75 positrons, which in turn corresponds to 0.55% of the scanned 50±7-Mev meson flux.

Multiple Events

Another method of estimating the positron flux makes use of multiple electron processes. Because of the scarcity of such events this method was not applied. The theory,[40] however, also predicts the number of positrons that will stop in the lead. For the conditions of this experiment 0.6% of the positrons will stop, thereby producing at most one (0.97) apparent meson stop.

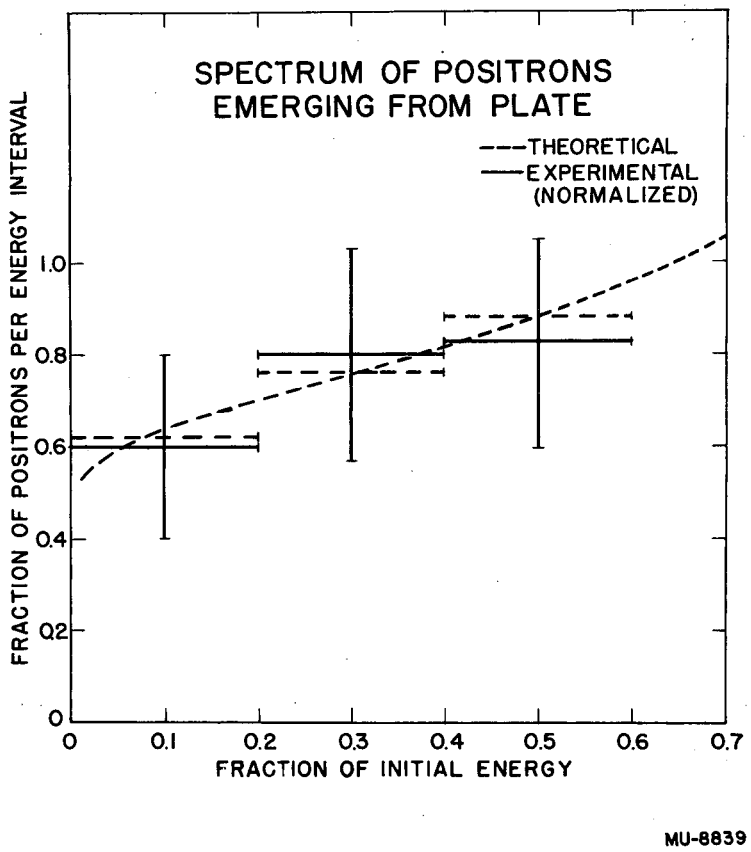
SPECTRUM OF POSITRONS
EMERGING FROM PLATE
---THEORETICAL
—EXPERIMENTAL
(NORMALIZED)
FRACTION OF POSITRONS PER ENERGY INTERVAL
1.0
0.8
0.6
0.4
0.2
0
0
0.1
0.2
0.3
0.4
0.5
0.6
0.7
FRACTION OF INITIAL ENERGY
MU-8839

Fig. 9

APPENDIX II

μ-Meson Contamination

The μ-meson contamination was calculated by considering the dynamics of the π - μ decay and taking into account the restrictions imposed by the collimators on the paths of μ-mesons. Several calculations were performed, using different simplifying assumptions. A value of 11% for the contamination was obtained each time. One such calculation is outlined below.

Approximations

The first collimator, actually 6.5 by 4 inches, is approximated by a circular hole 5 inches in diameter at a distance of 26 inches from a point source. Actually the source was a cylinder 2 inches in diameter and 2 inches long. The second collimator, located directly in front of the chamber, is taken at its actual value, 1 by 14 inches at a distance of 165 inches from the source. All the trajectories are considered to be straight lines.

Flux Emerging from First Collimator

Let the flux going in the proper direction for acceptance be limited to some angle δ. Since the meson flux has a $\cos^2\theta$ distribution[41] it is approximately constant at small angles, and the number of π-mesons in this acceptable flux is proportional to haversine δ.

The μ-meson flux originating before the first collimator and emerging through the 5-inch hole in the proper direction can be considered proportional to three factors:

1. The number of π-mesons traveling in a direction θ. This factor is $1/2 \sin\theta \, d\theta$ if the fluxes are normalized to unity.

2. The fraction of π-mesons decaying into μ-mesons before the collimator. This factor is essentially the possible distance traveled divided by the mean length for the π-mesons. For 45-Mev mesons this factor is given by the smaller of the quantities $(2.5/256)\csc\theta$ or $(26/256)\sec\theta$.

3. The fraction of μ-mesons going in the proper direction. This factor is given by $F(\theta)$ (haversine δ) $(1/2 \sin\theta)^{-1}$, where $F(\theta)$ is the fraction of μ-mesons given off at the angle θ. Because of the kinematics of the π-μ decay, two energies of the μ-meson are possible.

Those μ-mesons emitted in the backward hemisphere in the π-meson rest frame appear with too low radius of curvature to be accepted in the cloud chamber, thus only the forward decays in the π-meson rest frame need be considered. $F(\theta)$ is then the available fractional solid angle in the rest frame, and is given by $1/2 \sin \theta'$ where θ' is the angle corresponding to θ.

When these factors are combined, only Factor (2) and $1/2 \sin \theta' d\theta$ remain. When the integration is performed, a value of 3.1% is obtained. This number decreases slowly for higher π-meson energies.

Flux After First Collimator

For the region between the two collimators, the same reasoning is employed, but Factor (2) is modified from the approximate form x/x_o to the more accurate form $(1-e^{-x/x_o})$, where x is the distance available to the π-meson and x_o is the mean length for the meson. In this region an additional 2.0% of acceptable μ-mesons is produced.

Final Contamination

The total of 5.1% μ-mesons is calculated with respect to the original acceptable flux, of which only 47.5% reaches the chamber, the rest decaying into μ-mesons. Thus, with respect to the chamber flux the contamination is 10.7%.

Experimental Check

As a rough check on the purity of the meson beam, π-μ decays were noted during the scanning, and the number of such events was compared to the number expected for a pure π-meson beam. The result was a 12% contamination, accurate within a factor of two.

APPENDIX III

Effect of Meson Range on Apparent Angular Distribution

Weighting Factor for Normal Incidence

Let r be the range in lead of the meson that enters the plate of thickness t normal to its surface; let the meson be scattered through an angle θ at a distance x from the front surface of the plate. The meson will emerge from the lead plate if $x + (t-x)\sec\theta < r$.

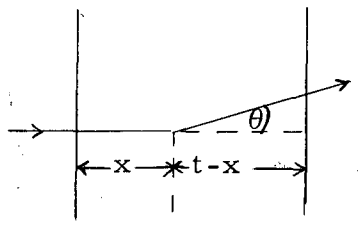

For any given scatter angle θ, the fraction of emergent mesons is given by $(t-x)/t$, where x is now the greatest lower bound of the set of values x which satisfy this inequality. Thus this fraction is simply $f(\theta) = (r/t - 1)/(\sec\theta - 1)$ for $\theta \geq \sec^{-1}(r/t)$

and $f(\theta) = 1$ for $\theta \leq \sec^{-1}(r/t)$.

Two methods of compensating for unobserved scatters are possible. Either each event is weighted by $f^{-1}(\theta)$ or an average weighting factor is used, such as the weight at the center point of the angular interval. For the data of this experiment both methods give the same result.

Weighting Factor for Nonnormal Incidence

For mesons entering at angles near 30° a different procedure was used to estimate the appropriate correction factor. It was assumed that mesons scattered into the plate at angles between an angle Δ and 90° (as measured from the normal) would be stopped in the plate. The angle Δ is defined by $\cos\Delta = t/2r$ and corresponds to the angle at which a meson will just reach the edge of the plate if it is scattered at the center. Thus for a fixed angle of incidence ($\alpha_i = 90^\circ$, $\beta_i = 30^\circ$) and a given scatter angle θ the limiting angles α_s can be found; the corresponding ϕ values are given by Eq. (5). The largest correction factor corresponded to the $60^\circ - 70^\circ$ and $110^\circ - 120^\circ$ intervals and was 1.77.

Only two large-angle scatters were observed among the mesons that entered near 15° to the plate normal. One of these required no correction factor; for the other, the weighting factor was taken as the average of the 0° and 30° factors.

APPENDIX IV

Illustrations of Events

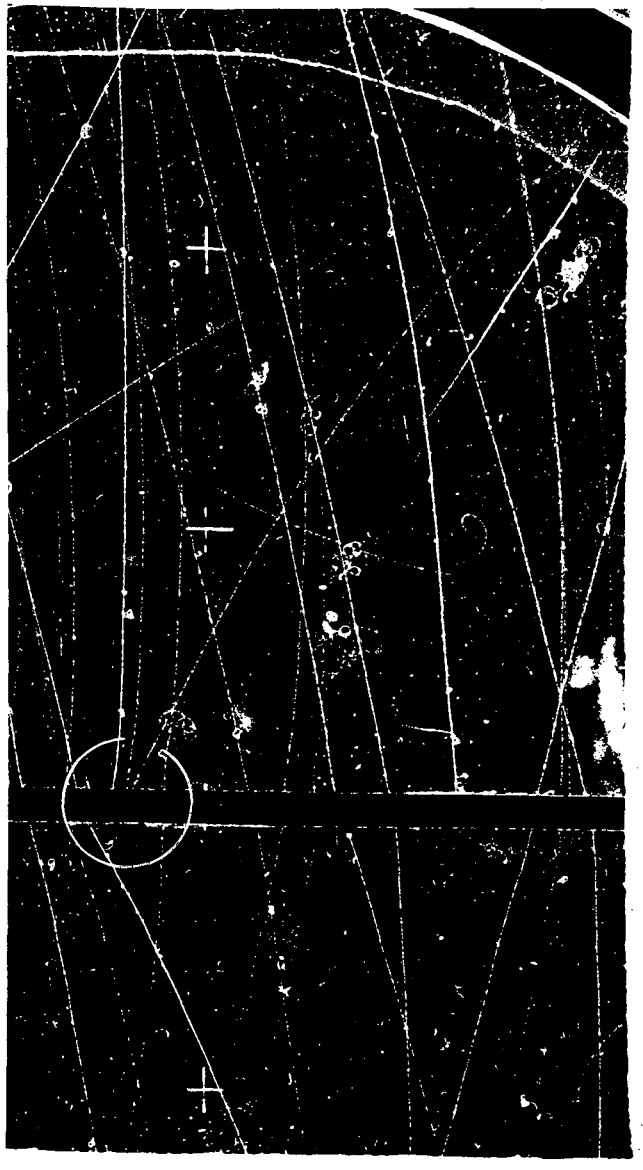

ZN-1086

Fig. 10. A 43-Mev meson scatters elastically through 163.5°. The magnetic field is 5.18 kilogauss.

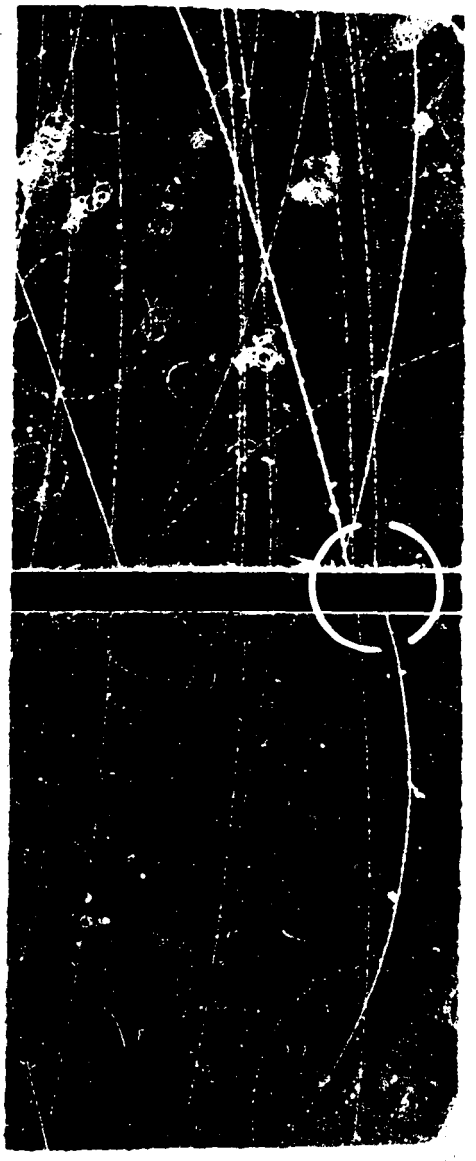

ZN-1087

Fig. 11. A 98-Mev π^+-meson is scattered inelastically through 29° and emerges from the lead plate with 2 Mev. The magnetic field is 5.18 kilogauss.

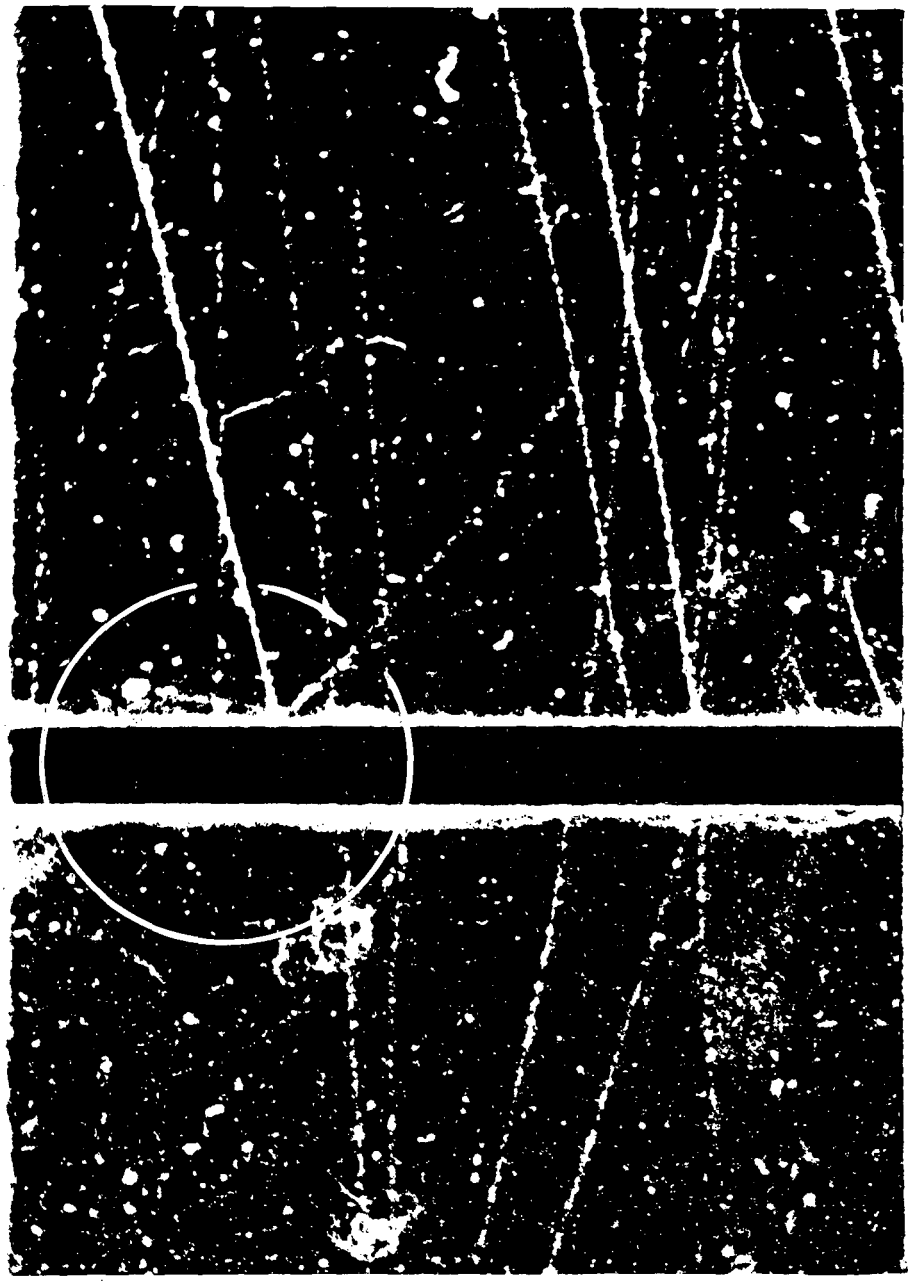

ZN-1088

Fig. 12. A 65-Mev meson scatters with charge exchange in the lead plate. The energy of the associated positron-electron pair is 64 Mev. The field is 5.18 kilogauss.

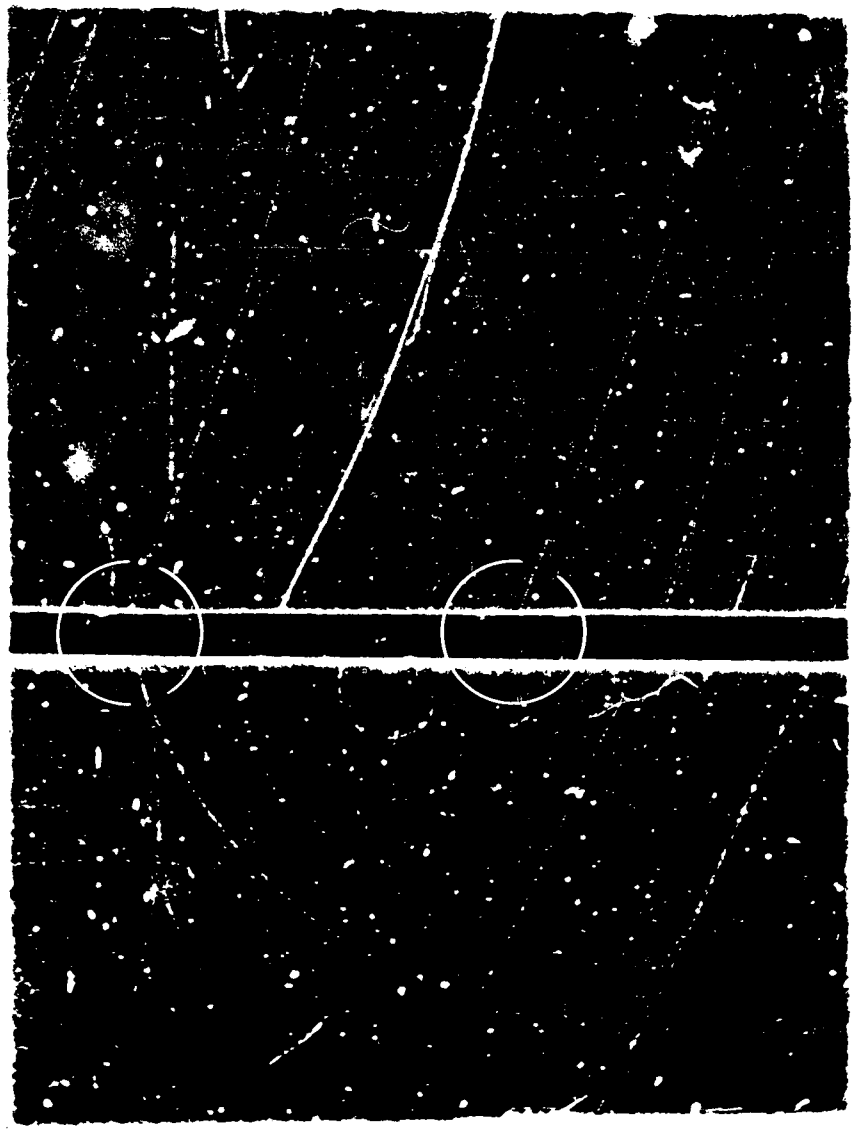

ZN-1089

Fig. 13. A 72-Mev meson scatters with charge exchange. The associated pair energy is 40.5 Mev. At the right, a 50-Mev meson stops in the plate. The field is 7.33 kilogauss.

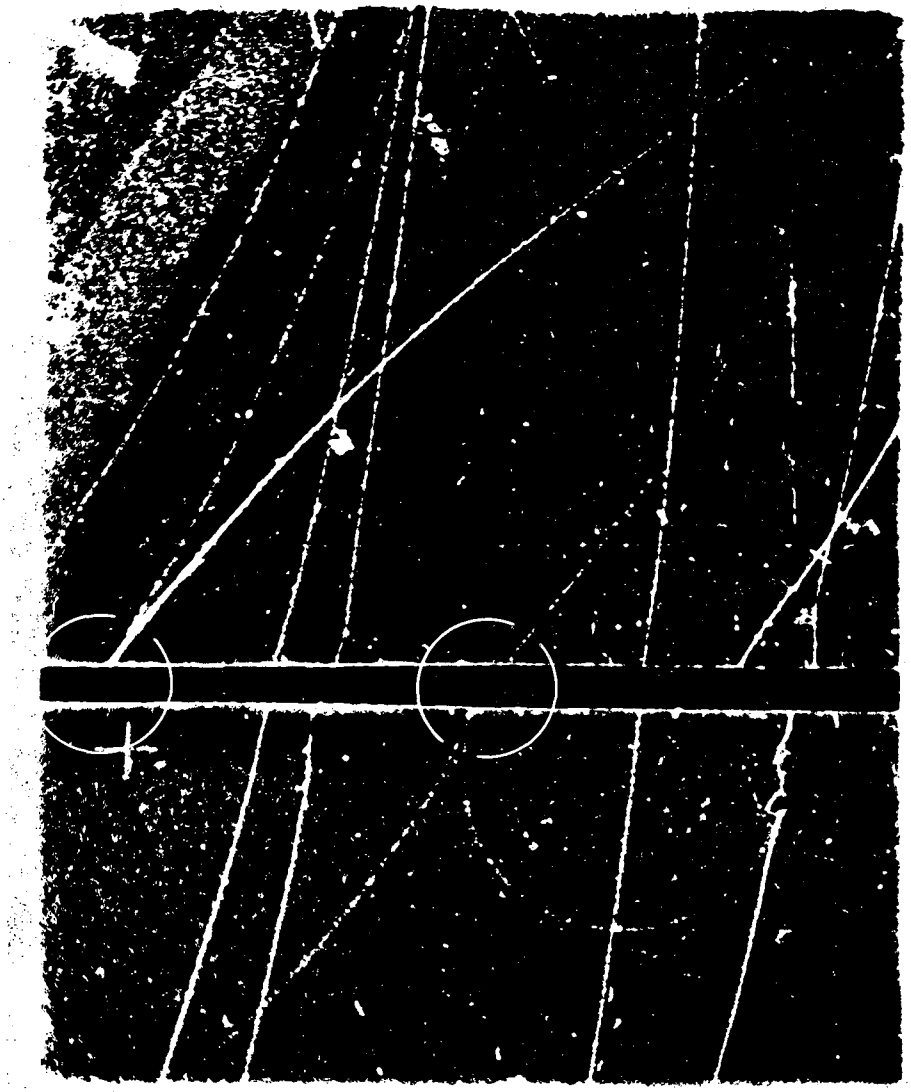

ZN-1090

Fig. 14. At the left, a 42-Mev π^+-meson produces a star in the lead. A 5.5-Mev proton emerges at 166.5°. Near the center a 111-Mev positron (or possibly a 39-Mev meson) produces a 60.5-Mev positron-electron pair at 19°. The field is 7.33 kilogauss.

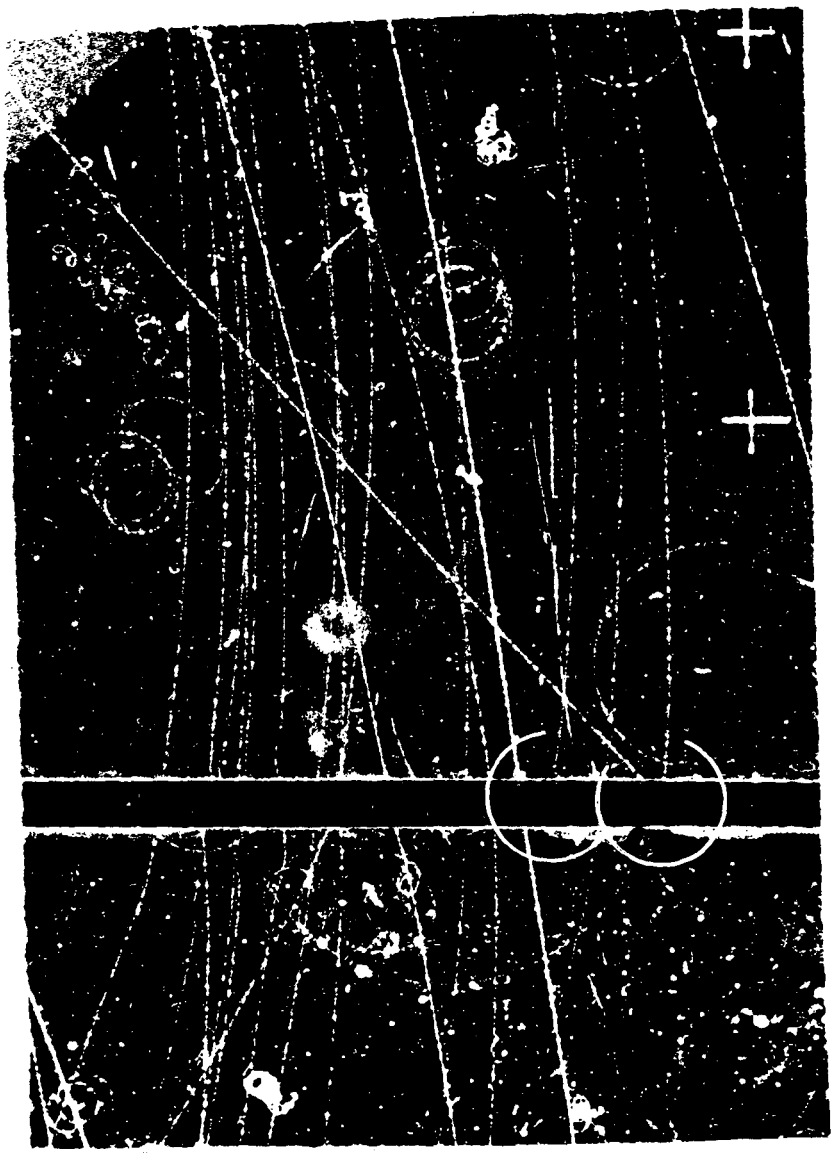

ZN-1091

Fig. 15. At the right, a 51-Mev meson is absorbed in the lead, and a 60-Mev proton emerges at 133°. Further to the left, a 37-Mev meson stops in the plate. The field is 5.18 kilogauss.

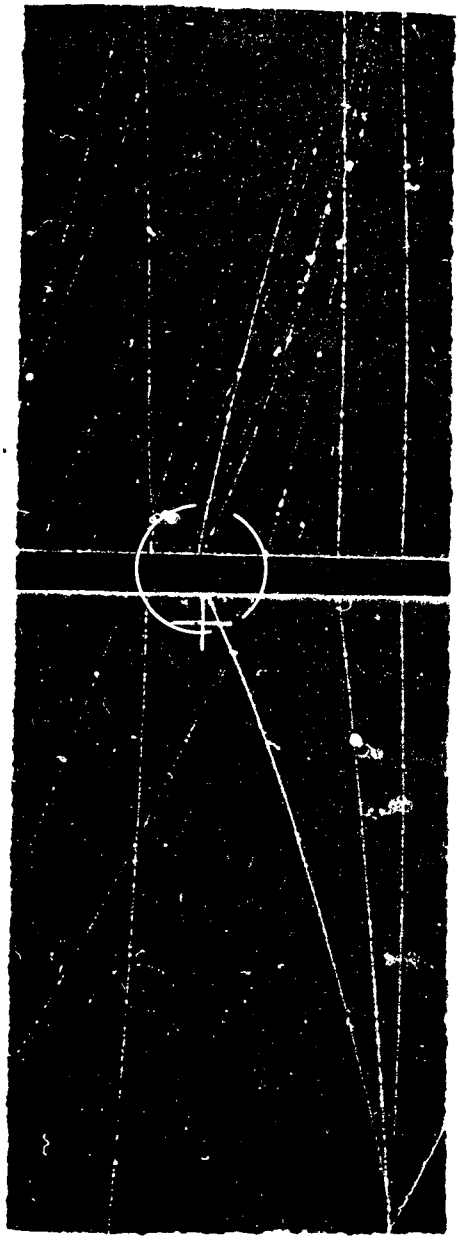

ZN-1092

Fig. 16. A 25-Mev meson is absorbed and two protons emerge. The energy of the forward proton is 12 Mev, of the backward proton 37 Mev. The angle between the protons is 148.5°. The magnetic field is 7.33 kilogauss.

REFERENCES

1. J. F. Tracy, Phys. Rev. 91, 960 (1953).
2. C. Richman, M. Skinner, J. Merritt, and B. Youtz, Phys. Rev. 80, 900 (1950).
3. W. M. Powell, Rev. Sci. Instr. 20, 403 (1949).
4. K. Brueckner, W. Hartsough, E. Hayward, and W. M. Powell, Phys. Rev. 75, 555 (1949).
5. W. Heitler, The Quantum Theory of Radiation, University Press, Oxford, 1949, p. 201, p. 225.
6. P. Lindenfeld, A. Sachs, and J. Steinberger, Phys. Rev. 89, 531 (1953).
7. J. Tinlot and A. Roberts, Phys. Rev. 95, 137 (1954).
8. B. Rossi and K. Greisen, Revs. Modern Phys. 13, 240 (1941).
9. E. C. Fowler, W. B. Fowler, R. P. Shutt, A. M. Thorndike, and W. L. Whittemore, Phys. Rev. 91, 135 (1953).
10. A. Pevsner, J. Rainwater, R. Williams and S. J. Lindenbaum, Phys. Rev. 94, 765 (1954); Phys. Rev. 91, 467 (1953).
11. F. H. Tenney and J. Tinlot, Phys. Rev. 92, 974 (1953).
12. H. Byfield, J. Kessler, and L. M. Lederman, Phys. Rev. 86, 17 (1952).
13. P. Isaacs, A. Sachs, and J. Steinberger, Phys. Rev. 85, 718 (1952).
14. A. Minguzzi, G. Puppi, and A. Ranzi, Nuovo cimento 11, 697 (1954).
15. G. Bernardini, E. T. Booth, L. Lederman, and J. Tinlot, Phys. Rev. 82, 105 (1951).
16. G. Bernardini, E. T. Booth, and L. Lederman, Phys. Rev. 83, 1277 and 1075 (1951).
17. H. Bradner and B. Rankin, Phys. Rev. 87, 553 and 547 (1952).
18. J. O. Kessler and L. M. Lederman, Phys. Rev. 94, 689 (1954).
19. H. H. Heckman and L. E. Bailey, Phys. Rev. 91, 1237 (1953).
20. H. L. Anderson, E. Fermi, R. Martin, and D. E. Nagle, Phys. Rev. 91, 155 (1953).
21. D. Bodansky, A. M. Sachs, and J. Steinberger, Phys. Rev. 93, 1367 (1954).
22. G. Bernardini and F. Levy, Phys. Rev. 84, 610 (1951).
23. A. Roberts and J. Tinlot, Phys. Rev. 90, 951 (1953).
24. W. J. Spry, Phys. Rev. 95, 1295 (1954).
25. R. Wilson and J. P. Perry, Phys. Rev. 84, 163 (1951).
26. C. Chedester, P. Isaacs, A. Sachs, and J. Steinberger, Phys. Rev. 82, 958 (1951).

27. R. L. Martin, Phys. Rev. 87, 1052 (1952).

28. K. J. Button, Phys. Rev. 88, 956 (1952).

29. M. W. Aarons, J. Ashkin, F. Feiner, J. G. Gorman, and L. Smith, Phys. Rev. 90, 342 (1953).

30. D. H. Stork, Phys. Rev. 93, 868 (1954).

31. S. Fernbach, R. Serber, and T. B. Taylor, Phys. Rev. 75, 1352 (1949).

32. D. H. Perkins, Phil. Mag. 40, 601 (1949).

33. K. A. Brueckner, R. Serber, and K. M. Watson, Phys. Rev. 84, 258 (1951).

34. M. Blau, A. R. Oliver, and J. E. Smith, Phys. Rev. 91, 949 (1953).

35. A. Bratenahl, S. Fernbach, R. H. Hildebrand, C. E. Leith, and B. J. Moyer, Phys. Rev. 77, 597 (1950).

36. M. G. K. Menon, H. Muirhead, and O. Rochat, Phil. Mag. 41, 583 (1950).

37. W. B. Cheston and L. J. B. Goldfarb, Phys. Rev. 78, 683 (1950).

38. F. L. Adelman, Phys. Rev. 85, 249 (1952).

39. R. Durbin, H. Loar, and J. Steinberger, Phys. Rev. 84, 581 (1951).

40. N. Arley, On the Theory of Stochastic Processes and their Application to the Theory of Cosmic Radiation, Gads Forlag, Copenhagen, 1948, p. 161-62.

41. W. F. Cartwright, C. Richman, M. N. Whitehead, and H. A. Wilcox, Phys. Rev. 91, 677, (1953).